Purdue University
Purdue e-Pubs

Birck and NCN Publications | Birck Nanotechnology Center

6-1-2008

Electrical detection of the biological interaction of a charged peptide via gallium arsenide junction-field-effect transistors

Kangho Lee
Purdue University

Pradeep R. Nair
Birck Nanotechnology Center, School of Electrical and Computer Engineering, Purdue University, pnair@purdue.edu

Muhammad A. Alam
Birck Nanotechnology Center, School of Electrical and Computer Engineering, Purdue University, alam@purdue.edu

David B. Janes
Purdue University, david.b.janes.1@purdue.edu

Heeyeon P. Wampler
Purdue University - Main Campus, park7@purdue.edu

See next page for additional authors

Follow this and additional works at: http://docs.lib.purdue.edu/nanopub

Lee, Kangho; Nair, Pradeep R.; Alam, Muhammad A.; Janes, David B.; Wampler, Heeyeon P.; Zemlyanov, Dmitry; and Ivanisevic, Albena, "Electrical detection of the biological interaction of a charged peptide via gallium arsenide junction-field-effect transistors" (2008). *Birck and NCN Publications.* Paper 162.
http://docs.lib.purdue.edu/nanopub/162

This document has been made available through Purdue e-Pubs, a service of the Purdue University Libraries. Please contact epubs@purdue.edu for additional information.

Authors
Kangho Lee, Pradeep R. Nair, Muhammad A. Alam, David B. Janes, Heeyeon P. Wampler, Dmitry Zemlyanov, and Albena Ivanisevic

This article is available at Purdue e-Pubs: http://docs.lib.purdue.edu/nanopub/162

Electrical detection of the biological interaction of a charged peptide via gallium arsenide junction-field-effect transistors

Kangho Lee,[1] Pradeep R. Nair,[1] Muhammad A. Alam,[1] David B. Janes,[1,a)] Heeyeon P. Wampler,[2] Dmitry Y. Zemlyanov,[3] and Albena Ivanisevic[2,a)]
[1]*School of Electrical and Computer Engineering, The Institute for Nanoelectronics and Computing, and Birck Nanotechnology Center, Purdue University, West Lafayette, Indiana 47907, USA*
[2]*Department of Chemistry and Weldon School of Biomedical Engineering, Purdue University, West Lafayette, Indiana 47907, USA*
[3]*Birck Nanotechnology Center, Purdue University, West Lafayette, Indiana 47907, USA*

(Received 8 September 2007; accepted 25 March 2008; published online 11 June 2008)

GaAs junction-field-effect transistors (JFETs) are utilized to achieve label-free detection of biological interaction between a probe transactivating transcriptional activator (TAT) peptide and the target trans-activation-responsive (TAR) RNA. The TAT peptide is a short sequence derived from the human immunodeficiency virus-type 1 TAT protein. The GaAs JFETs are modified with a mixed adlayer of 1-octadecanethiol (ODT) and TAT peptide, with the ODT passivating the GaAs surface from polar ions in physiological solutions and the TAT peptide providing selective binding sites for TAR RNA. The devices modified with the mixed adlayer exhibit a negative pinch-off voltage (V_P) shift, which is attributed to the fixed positive charges from the arginine-rich regions in the TAT peptide. Immersing the modified devices into a TAR RNA solution results in a large positive V_P shift (>1 V) and a steeper subthreshold slope (~ 80 mV/decade), whereas "dummy" RNA induced a small positive V_P shift (~ 0.3 V) without a significant change in subthreshold slopes (~ 330 mV/decade). The observed modulation of device characteristics is analyzed with analytical modeling and two-dimensional numerical device simulations to investigate the electronic interactions between the GaAs JFETs and biological molecules. © *2008 American Institute of Physics*. [DOI: 10.1063/1.2936853]

I. INTRODUCTION

With continuous advances in discovering biomarkers for specific diseases, the field of chemical sensors, particularly biosensors, has been receiving enormous attention. In particular, recent discoveries of several cancer markers in external human secretions could allow the development of techniques to detect cancers without a biopsy in the early stages of the disease.[1] Generally, a biochemical sensor consists of two parts: (1) an interactive "probe" molecule, which is reactive to the analytes in the enviroment and generates a response, and (2) a transduction device (e.g., a transistor) that reads the response and converts it into a quantifiable signal. Various transduction devices that utilize biological molecules as interactive materials have been demonstrated on the basis of different transduction mechanisms, including quartz crystal microbalances for mass change detection, quantum dots linked to DNA probes for fluorescence signal change detection, nanowire transistors for net surface charge modulation detection, and electromechanical systems with nanoscale structures such as cantilevers for detection of static deflections or shifts in resonant frequency.[2–5] Among these devices, electrical transducers based on semiconductor electronic devices are considered as promising candidates due to their ease of miniaturization, integration into microelectronic circuits, and label-free detection, which will enable mobile biosensor devices for real-time monitoring of critical clinical parameters or on-demand detection of diseases.

The first implementation of conduction-based chemical sensors can be traced back to an ion-sensitive field-effect transistor (ISFET) *p*H sensor, which is a Si-based metal-oxide-semiconductor field-effect transistor (MOSFET) with its gate replaced by a reference electrode inserted in an electrolyte solution that is in direct contact with the gate oxide.[6] Polycrystalline Si thin-film transistors with a Si_3N_4 gate insulator in the device configuration similar to ISFET have been recently utilized to demonstrate detection of DNA hybridization.[7] Although nanowire devices could provide higher sensitivity, such planar structures are expected to allow better quantitative understanding of the mechanisms of channel modulation due to molecular-level events.

One of the prerequisites in developing electrical transducers based on semiconductor devices is a reliable surface modification that provides not only a selective binding layer for target species but also a blocking layer for nontarget species (e.g., polar ions in physiological solutions) that may induce nonspecific background signals. In particular, since semiconductor surfaces functionalized only with bulky biomolecules are likely to have a large amount of vacant sites, surface passivation methodologies compatible with chemically sensitive biomolecules need to be considered when developing biomembranes for conduction-based biosensors. In the case of Si, electrically well-defined insulating materials such as Si_3N_4 have been used to passivate the Si surface from direct exposure to target analyte solutions and subse-

[a)]Authors to whom correspondences should be addressed. Electronic addresses: janes@ecn.purdue.edu and albena@purdue.edu.

 © 2008 American Institute of Physics

Downloaded 20 Nov 2008 to 128.46.220.88. Redistribution subject to AIP license or copyright; see http://jap.aip.org/jap/copyright.jsp

quently modified with molecules of interest.[7] However, direct electrostatic interactions between biomolecules and semiconductor surfaces will be suppressed by an insulating material in between. In addition, surface modification of the insulating material is limited by viable surface chemistry and typically requires additional linker molecules, which may lead to reduction in sensitivity. A more generic way would be to utilize molecular passivation of semiconductor surfaces with biomolecules inserted into or anchored on the passivating layer, i.e., chemically sensitive molecular passivation. Studies on conformation and surface coverage of diverse organic molecules self-assembled on various semiconductor surfaces are expected to provide approaches for developing chemically sensitive molecular passivation.[8–12] In particular, strong covalent bonding of thiolated molecules on GaAs surfaces makes GaAs an attractive substrate for biosensor platforms because numerous biomolecules can be easily modified with thiols for surface functionalization.

In this study, GaAs junction-field-effect transistors (JFETs) are fabricated to investigate the effects of organic adsorbates on electrical device characteristics and used to demonstrate electrical detection of a biological interaction between transactivating transcriptional activator (TAT) peptide, a short peptide sequence derived from the human immunodeficiency virus-type 1 TAT protein, and the transactivation-responsive (TAR) RNA. The specific peptide and RNA in this study were chosen based on the high binding affinity between the TAT peptide and the stem-loop region of the TAR-RNA,[13] which provides relatively stable and reproducible device characteristics. In addition, this peptide contains a relatively large net positive charge, which is partially compensated upon binding by the charge on the RNA. Therefore, the peptide/RNA pair provides a relatively well understood model system for biosensor applications involving species containing net or induced charge. The device structure has been chosen to provide relatively close coupling between the molecular species and the channel, as well as an effective back gate to allow quantification of the effects from both fixed and voltage-variable charge states. As will be shown later, exposing the as-fabricated devices to physiological solutions degrades gate modulation effects and significantly decreases the channel conductivity, which indicates that the chemically sensitive molecular passivation needs to be incorporated into GaAs-based biosensors before exposure to target analyte solutions. Here, we also demonstrate that mixed adlayers of 1-octadecanethiol (ODT) and TAT peptide, formed by sequential solution-cast self-assembly, provide effective molecular passivation and enable electrical detection of the binding of TAT peptide to TAR RNA.

II. EXPERIMENT

A. Device fabrication

The GaAs JFET device structure is shown in Fig. 1, along with the amino acid sequence of a TAT peptide. The device structure has been designed to allow subthreshold behavior to be observed for relevant ranges of surface charges or dipoles for high sensitivity. The epilayer structure consists

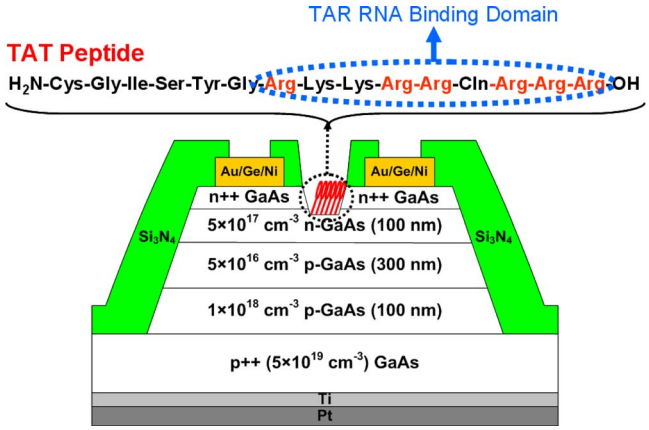

FIG. 1. (Color online) Cross-sectional device structure of a GaAs JFET with the amino acid sequence of TAT peptide. The arginine-rich TAR RNA-binding domain composed of nine amino acids is indicated in a dotted circular box.

of a 100 nm heavily doped (2×10^{19} cm^{-3}) n-GaAs layer for low contact resistance, a 100 nm Si-doped (5×10^{17} cm^{-3}) n-GaAs channel layer, a 300 nm Be-doped (5×10^{16} cm^{-3}) p-GaAs layer for gate modulation via p-n-junction depletion width changes, and a 100 nm Be-doped (1×10^{18} cm^{-3}) p-GaAs low-resistance buffer layer, all of which are grown on a p^{++} GaAs (5×10^{19} cm^{-3}) substrate by molecular beam epitaxy. Device isolation was achieved by conventional photolithography and mesa etching with a mixture of $H_2SO_4/H_2O_2/H_2O$. Next, a common gate contact was formed on the back side by e-beam deposition of Pt (50 nm)/Ti (10 nm) at $\sim5\times10^{-7}$ Torr (deposition rate=1 Å/s). Source/drain Ohmic contacts were defined by e-beam deposition of Au/Ge/Au/Ni/Au films and lift-off, followed by 400 °C rapid thermal annealing in an N_2 ambient for 30 s. Specific contact resistivity, measured by the transfer length method, was $\sim1\times10^{-6}$ Ω cm. A 300 nm layer of Si_3N_4 was then deposited for device passivation by plasma-enhanced chemical vapor deposition. Active device and contact regions were defined by conventional photolithography and exposed by dry etching the Si_3N_4 layer using a SF_6/O_2-based plasma reactive ion etch. Finally, recess etching was performed to adjust the pinch-off voltage (V_P) by wet etching the n-GaAs layers with a mixture of $NH_4OH/H_2O_2/H_2O$, where V_P is defined as the gate voltage for which the JFET channel is completely depleted. The length and width of the recess, 2 and 200 μm, respectively, determine the device dimension. The current-voltage characteristics of the "as-fabricated" devices were measured in air by using a Keithley 4200 semiconductor parameter analyzer.

B. Surface preparation

Prior to molecular deposition, the devices were cleaned in acetone, isopropyl, and pure ethanol and dried with nitrogen, followed by 1 min concentrated HCl cleaning to remove the native GaAs oxide. The TAT peptide sequence containing an arginine-rich RNA-binding domain was synthesized by AnaSpec (San Jose, CA). For ODT modification, the devices were immersed in a 1 mM ODT solution in ethanol (ETH) for 24 h at room temperature. For TAT peptide modification,

Downloaded 20 Nov 2008 to 128.46.220.88. Redistribution subject to AIP license or copyright; see http://jap.aip.org/jap/copyright.jsp

the devices were incubated in a 1 mM TAT peptide solution in phosphate-buffered saline (PBS) at pH ~ 7.3 for 24 h at 4–8 °C. A mixed adlayer of ODT and TAT peptide was formed by sequential solution-cast self-assembly of 1 mM ODT in dimethylformamide (DMF) and 1 mM TAT peptide in DMF, following the same procedure for each reagent. DMF was used to prevent the devices from being exposed to polar ions in PBS. Next, the samples were rinsed several times with a corresponding base solvent (ETH, DMF, or PBS) and dried with nitrogen, and the electrical characteristics of the modified devices were measured in air. The details of the adlayer deposition and subsequent surface analysis have been described previously.[14] For comparable deposition parameters, the surface coverages of the various layers were estimated to be approximately 1 monolayer (ML) for the ODT layer, 4% of a monolayer for the TAT peptide layer, and 0.7 ML for the mixed adlayer (with the TAT peptide representing approximately 2% of a monolayer, corresponding to $\sim 3 \times 10^{13}$ molecules/cm^2).[14] The identical TAT peptide sequence attached on the GaAs surface is known to retain its original biorecognition property and interact with TAR RNA via the arginine-rich RNA-binding domain.[9] The devices functionalized with the mixed adlayer were immersed in either a TAR RNA solution or a dummy RNA solution for 3 h in order to verify the reactivity of TAT peptides in the mixed adlayer with TAR RNA. The TAR RNA sequence (5′-GGC CAG AUC UGA GCC UGG GAG CUC UCU GGC C-3′) and the dummy RNA sequence (5′-AGA CAG AUA AGA ACA AGA AGG AUA ACA AGA A-3′) were synthesized, purified, and analyzed by Integrated DNA Technologies (Coralville, IA). The 5 μM solutions of TAR RNA and dummy RNA were prepared in tris-EDTA buffer at pH ~ 8.0. After rinsing the samples with the same buffer, washing copiously with ultrapure water, and drying under nitrogen, electrical characteristics of the devices were measured in air.

In order to investigate the surface chemical composition and confirm the presence of the TAT peptide in the mixed adsorption layer, x-ray photoelectron spectroscopy (XPS) was used after the various adsorption steps. XPS data were obtained by a Kratos Ultra DLD spectrometer using monochromatic Al $K\alpha$ radiation ($h\nu$=1486.58 eV). The survey and high-resolution spectra were collected at fixed analyzer pass energies of 160 and 20 eV, respectively. The spectra were collected at 0° angle with respect to the surface normal. The atomic concentrations of the chemical elements in the near-surface region were estimated after the subtraction of Shirley-type background, taking into account the corresponding Scofield atomic sensitivity factors and inelastic mean free path of photoelectrons as a standard procedure of CASAXPS software. The binding energy (BE) values referred to the Fermi level were corrected using the C 1s 284.80 eV. A commercial Kratos charge neutralizer was used to achieve a resolution of 0.6–0.7 eV measured as a full width at half maximum of the As 3d and Ga 3d deconvoluted spin-orbital split doublets. The XPS spectra were fitted by CASAXPS software assuming the line shape to be a Gaussian–Lorentzian function.

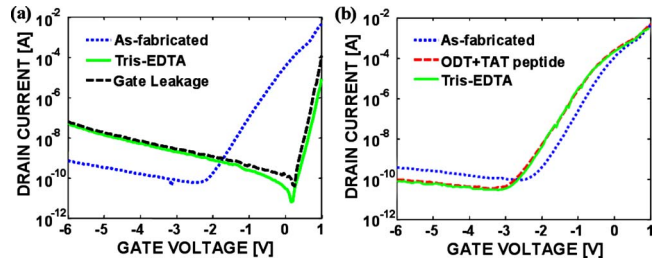

FIG. 2. (Color online) Transfer characteristics of (a) an as-fabricated device before and after immersion in tris-EDTA buffer; gate leakage current is also shown and (b) a device modified with the mixed adlayer before and after immersion in tris-EDTA buffer. V_{DS} was set to 0.1 V.

III. RESULTS AND DISCUSSION

A. Surface characterization

Figures 2 and 4 show transfer characteristics (drain current versus gate-to-source voltage) at a drain-to-source voltage of 0.1 V for representative devices in both the as-fabricated state and following the specified molecular depositions on the same devices. The as-fabricated devices exhibited typical depletion-mode I-V characteristics with a V_P of −1.5 V. The low subthreshold slope (S_{sub}) for the as-fabricated devices indicates the presence of significant amount of interface charges (N_{IT}). As shown in Fig. 2(a), immersing the devices in tris-EDTA buffer for 24 h resulted in an enormous conductivity reduction and a near-complete elimination of gate modulation of the device conductivity, presumably due to the presence of significant negative charges on the surface; comparable effects were observed following the immersion in PBS. A current kink above zero gate bias observed in Fig. 2(a) is due to forward-biased p-n junction current between the gate and the source/drain. Direct modification of the surface with TAT peptides in PBS resulted in a conductivity collapse similar to that in Fig. 2(a), whereas the devices modified with TAT peptides in DMF retained their original conductivity and gating characteristics, with a positive V_P shift as large as 0.3 V (data not shown). It is speculated that the n-type GaAs channel layer becomes completely depleted by negative phosphate ions from PBS solution sitting on the GaAs surfaces when immersed in the buffer solutions—indeed, the existence of phosphates on the GaAs surfaces has been verified by XPS. To prevent such parasitic surface adsorption of phosphate ions, a mixed adlayer of ODT and TAT peptide was deposited in DMF; Fig. 2(b) shows the transfer characteristics for a device modified with the mixed adlayer. In this case, the I-V characteristics shifted modestly following mixed adlayer formation, but remained essentially unchanged after subsequent exposure to tris-EDTA buffer, which indicates that the mixed adlayer passivates the GaAs surface from polar ions in buffer solutions. A negative V_P shift observed upon the mixed adlayer formation is attributed to the positive charges ($+qN_{OT}^{(TAT)}$) on the TAT peptides. While the TAT peptide is completely protonated in buffer solutions, it is not clear that they are completely protonated in air. The negligible response to the

Downloaded 20 Nov 2008 to 128.46.220.88. Redistribution subject to AIP license or copyright; see http://jap.aip.org/jap/copyright.jsp

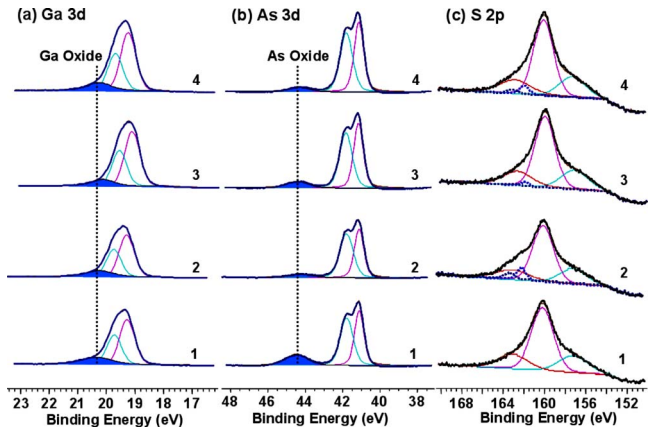

FIG. 3. (Color online) XPS high-resolution spectra for (a) Ga 3*d*, (b) As 3*d*, and (b) S 2*p*: (1) cleaned GaAs, (2) GaAs functionalized with ODT, (3) GaAs functionalized with the TAT peptide, and (4) GaAs functionalized with the mixed adlayer of ODT and TAT peptide.

buffer solution indicates that stable molecular passivation is realized by using the mixed adlayer.

As further verification that the surface has been passivated by ODT and decorated with TAT peptides, Fig. 3 shows the core-level spectra (Ga 3*d*, As 3*d*, and S 2*p*) obtained for (1) GaAs cleaned in HCl, (2) GaAs functionalized with ODT, (3) GaAs functionalized with the TAT peptide, and (4) GaAs functionalized with the mixed adlayer of ODT and TAT peptide. The peaks characterizing Ga_2O_3 (20.3 eV) and As_2O_3 (~44.5 eV) were detected after etching in HCl, which is attributed to surface oxidation in air during transfer to the XPS spectrometer. After immobilization of ODT, the oxide amount decreased, especially As_2O_3, which was hardly detectable. To quantitatively determine the oxidation states on the surface, we collected Ga 2*p* and As 2*p* spectra (supporting information) due to their higher surface sensitivity than Ga 3*d* and As 3*d*. This increase in sensitivity is due to the electron attenuation lengths, for Ga $2p_{3/2}$ and As $2p_{3/2}$, which are 0.859 and 0.525 nm, respectively, whereas the corresponding values for Ga 3*d* and As 3*d* are 2.61 and 2.57 nm. Based on the As $2p_{3/2}$ and As 3*d* spectra, the GaAs surface is more easily oxidized when functionalized with the mixed adlayer of ODT and TAT peptide than with the homogeneous ODT monolayer. The S 2*p* core-level peak overlaps with Ga 3*s*, therefore to extract the data on the S 2*p* peak, curve fitting was used, as shown in Fig. 3(c). A single doublet, which is characterized by the BE of approximately 162 eV for S $2p_{3/2}$, was observed after functionalizing the surface with homogeneous and mixed adlayers, which verifies a covalent bond formed between the thiol group and the surface. Even though N 1*s* spectra could provide a clear evidence for the existence of the TAT peptides on the GaAs surface, it is difficult to determine the amount of amide N on the surface from the N 1*s* spectra due to the overlap with Ga Auger peaks. The presence of the hydrocarbons on the surface is evaluated with the C 1*s* spectra; the peak positions and their assignments are summarized in Table I. Carbon atoms in the TAT peptide structure can be in one of six chemical positions: (1) carbon bonded only to carbon and/or hydrogen, (2) carbon coordinated with one nitrogen atom along with carbon and/or a hydrogen atom, (3) carbon atom with a single bond to an oxygen atom, (4) carbon from an amide group, (5) carbon atom with a double bond to oxygen atom, and (6) carbon coordinating with three nitrogen atoms, as in arginine. The carbon atoms in these six moieties are expected to have different chemical shifts, and the intensity of the individual components is expected to be proportional to the population of the particular carbon type. Amide C species are observed on the TAT peptide treated surfaces, and all carbon species of the TAT peptide and ODT are observed on ODT/TAT peptide mixed adlayer surfaces. The presence of amide C and C–N species confirmed the attachment of the TAT peptides on the GaAs surfaces.

TABLE I. BE of different components of C 1*s* peak obtained after the face was functionalized with ODT, TAT peptide, and a mixed adlayer of ODT and TAT peptide.

Surface	BE (eV)	Relative area of C 1*s* components (%)	Peak assignment
ODT	284.8	93.2	C–C and C–H
	285.9	6.8	C–O[a]
TAT Peptide	284.8	15.2	C–C and C–H (TAT)
	286.4	11.3	C–N and C–O (TAT)[b]
	288.2	8.4	Amide C and C=O(TAT)[c]
	289.6	3.0	Arginine (TAT)
	285.0	62.1	Residual hydrocarbons
Mixed Adlayer (ODT/TAT Peptide)	284.8	8.2	C–C and C–H (TAT)
	286.5	6.1	C–N and C–O (TAT)
	288.1	4.5	Amide C and C=O(TAT)
	289.7	1.6	Arginine (TAT)
	285.0	79.7	C–C and C–H (ODT)

[a]Due to residual hydrocarbons appeared during sample transfer through atmosphere.
[b]For simplicity carbon atoms bond to nitrogen and oxygen were fitted with one peak.
[c]For simplicity carbon atoms from amide group and double bond to oxygen were fitted with one peak.

Downloaded 20 Nov 2008 to 128.46.220.88. Redistribution subject to AIP license or copyright; see http://jap.aip.org/jap/copyright.jsp

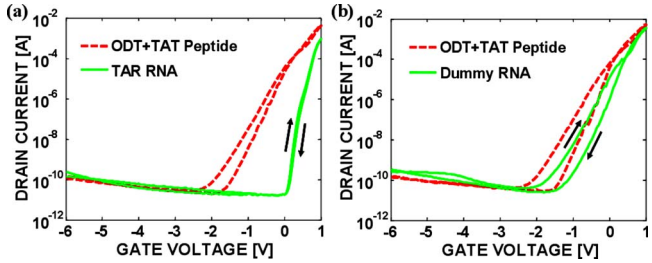

FIG. 4. (Color online) Transfer characteristics of GaAs JFET devices modified with the mixed adlayer before and after reaction with (a) TAR RNA (b) "dummy" RNA. Forward and backward sweeps are indicated by arrows, and the sweeping rate of the gate bias was 600 mV/s. V_{DS} was set to 0.1 V.

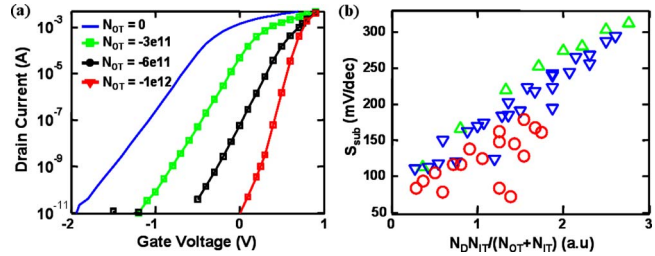

FIG. 5. (Color online) Device simulations indicating the effect of surface adsorbed charges for the device schematic shown in Fig. 1. (a) Effect of varying adsorbed surface charge density (N_{OT}) with interfacial trap density (N_{IT}) set to 1×10^{12} eV^{-1} cm^{-2}. As the magnitude of surface adsorbed charges is increased, the S_{sub} improves along with the change V_{th}. (b) Linear correlation between S_{sub} and $N_D N_{IT}/(N_{OT}+N_{IT})$ with different channel doping densities (N_D) values of $N_D=4\times10^{17}$ cm^{-3} (triangles), $N_D=3\times10^{17}$ cm^{-3} (inverted triangles), and $N_D=2\times10^{17}$ cm^{-3} (circles).

B. Capture of "target" TAR RNA and numerical analysis

Figure 4 shows the transfer characteristics of representative devices functionalized with the mixed adlayers before and after reaction with either TAR RNA or dummy RNA, demonstrating specific electrical detection of TAT peptide-TAR RNA interactions. While previous attempts to electrically detect biomolecules involved either a change in conductivity[4] or a shift in threshold voltage,[7] TAR RNA immobilized on the devices induced distinctive changes in V_P, S_{sub}, and *I-V* hysteresis. A primary mechanism behind TAT peptide-TAR RNA interactions is the electrostatic attraction between protonated TAT peptides ($+qN_{OT}^{(TAT)}$) and TAR RNA with negative charges on the phosphate backbone, $-qN_{OT}^{(TAR)}$ ($q=1.6\times10^{-19}$ C). Hence, a large positive V_P shift (>1 V) observed in the TAR RNA-modified devices is attributed to an increase in surface depletion width due to net surface negative charges from TAR RNA bonded to TAT peptides in the mixed adlayer ($+qN_{OT}^{(TAT)}-qN_{OT}^{(TAR)}$), whereas a small positive V_P shift (~0.3 V) is thought to be induced by a small amount of dummy RNAs physisorbed on the GaAs surface after rinsing with buffer.

Surprisingly, the surface immobilization of TAR RNA significantly improves S_{sub} to ~80 mV/decade, in contrast to ~330 mV/decade from either as-fabricated or dummy RNA-modified devices. Typical MOSFET analyses relate the improvement in S_{sub} to a reduction of surface states ($S_{sub}\sim2.3\ k_BT/q(1+C_{it}/C_{ox})$), hence the reduction in S_{sub} should be due to reduction in C_{it} (the capacitance due to surface states).[15] However, TAR RNA is not expected to reduce C_{it}, so the improvement in S_{sub} is counterintuitive. The resolution of this puzzle lies in the distinction between inversion-mode (MOSFET) and depletion (JFET) devices.

In inversion-mode devices, it is well established that S_{sub} is related to the rate of increase of minority carriers in the channel with the gate voltage.[15] Hence, the presence of surface states always degrades (i.e., increases) S_{sub}. However, in depletion-mode devices, S_{sub} is associated with the amount of majority carriers that the gate is required to deplete. For a given doping and device dimensions, any external factors which help to lower the integrated amount of majority carriers in the device result in steeper S_{sub}.This is clearly illustrated with the help of numerical simulations[16] in Fig. 5. Here, we solve semiclassical drift diffusion equations along with the Poisson's equation in two dimensions to study the effects of surface states and adsorbed surface charges on the GaAs JFET response. Figure 5(a) indicates that as the magnitude of surface charge density $|-qN_{OT}^{(TAR)}|$ is increased from 0 to 10^{12} cm^{-2}, the S_{sub} of the JFET devices improves. In contrast, for inversion-mode devices, such increase in $|-qN_{OT}^{(TAR)}|$ would have resulted in just a parallel shift of *I-V* characteristics. The simulation results consistently explain the experimental V_P shift and the improvement of S_{sub} (Fig. 4) and indicate that it is the negative charges on the RNA that results in this behavior. The improvement in subthreshold characteristics is due to dependence of the rate of change of peak channel potential on the electric field at the ODT-GaAs interface. Increase in N_{OT}, the effective surface charge density due to adsorbed molecules, for a given interfacial trap density (N_{IT}), results in a larger rate of reduction of peak channel potential and hence the S_{sub} improves.

The numerical interpretation discussed above can be also encapsulated in the following analytical result:

$$S_{sub}=2.3\frac{k_BT}{q}\left[(1-D)\left(1+D\frac{|N_{OT}|}{N_Dt}\right)+\frac{D^2\alpha}{N_Dt}\right]^{-1}. \qquad (1)$$

Here, t, N_D, and ε are the thickness, doping, and dielectric constant of the *n*-GaAs layer, respectively. Also, $D\equiv qN_{it}/(qN_{it}+\varepsilon/t)$ and $\alpha=(\varepsilon kT/qt)\ln(N_VN_D/n_i^2)+(\varepsilon V_G/qt)+N_Dt$, where N_V is the valence-band density of states and n_i is the intrinsic carrier concentration. Equation (1) reduces to classical limits in which (a) $S_{sub}=2.3\ k_BT/q$ with $N_{IT}=0$, $N_{OT}=0$, and (b) S_{sub} increases with increasingly N_{IT}, given that $N_{OT}=0$. In addition, Eq. (1) also interprets the counterintuitive decrease in S_{sub} with increasing N_{OT} (and nonzero N_{IT}) as discussed in this paper. Finally, note that for large N_{IT} and N_{OT} (N_{OT}(cm^{-2}), N_{IT}(cm^{-2} eV^{-1})$>10^{11}$), S_{sub} of the back-gated depletion-mode devices follows the scaling relationship $S_{sub}\approx f(N_DN_{IT}/(N_{OT}+N_{IT}))$, as confirmed by numerical simulations in Fig. 5(b).

The hysteresis in *I-V* characteristics after dummy RNA detection [Fig. 4(b)] can also be qualitatively explained on the basis of Eq. (1) as well as the simulation results shown in Fig. 5. Since the as-fabricated devices exhibited negligible hysteresis, it is speculated that during the forward gate voltage sweep, electrons are trapped in states within the TAT

Downloaded 20 Nov 2008 to 128.46.220.88. Redistribution subject to AIP license or copyright; see http://jap.aip.org/jap/copyright.jsp

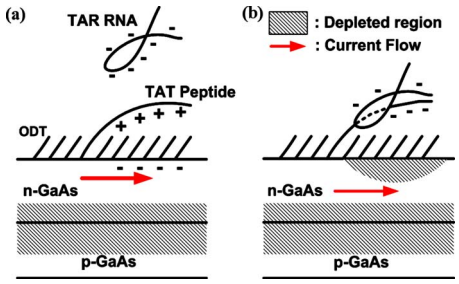

FIG. 6. (Color online) A proposed sensing mechanism. (a) The device modified with the mixed adlayer before reaction with TAR RNA. (b) Conjugation of the TAT peptide and TAR RNA results in net negative surface charges, inducing surface depletion regions. Reduction in effective channel thickness gives rise to the positive pinch-off voltage shift. Also, the conduction path in the channel is pushed more into the bulk of the device, substantially reducing the interaction with the surface states, and accordingly, resulting in negligible hysteresis.

peptides. These trapped electrons act as a net negative surface charge during the reverse gate voltage sweep. As discussed earlier, negative surface charge results in V_P shift and improved S_{sub}, resulting in a different path during the reverse sweep, i.e., hysteresis. On the other hand, after TAR RNA surface immobilization, current conduction occurs deeper inside the channel, and hence lowers the probability of carrier trapping in the surface monolayer, which results in practically zero hysteresis. The mechanism that induces modification of the device characteristics (V_P, S_{sub}, and hysteresis) is illustrated in Fig. 6.

Our results provide an interesting observation regarding the sensitivity of nanosensors in detecting biomolecules. Generally, it is regarded that nanoscale devices are more sensitive to biomolecules since their size is comparable to that of the biomolecules themselves. Here, we propose that even by using devices whose dimensions are in the micrometer regime, highly sensitive detection is possible by optimum design of operating conditions. Based on the device simulations, N_{OT} of -5×10^{12} cm^{-2} is required for the observed experimental shift in *I-V* characteristics due to TAR RNA conjugation. In the buffer solution, a TAR RNA molecule, by itself, is expected to have $-30q$, assuming that a phosphodiester linkage in RNAs has $-1q$, where q is the electron charge. Even though it is theoretically possible to evaluate net surface charges ($Q_{S,\text{RNA}}$) due to a conjugated TAR RNA by solving the nonlinear Poisson–Boltzmann equation numerically in a given geometry,[17,18] the boundary conditions and the ion concentration to be used are not well defined because the measurements were performed in air after draining out the buffer solution. $Q_{S,\text{RNA}}$ is thought to be much less than $-30q$ because of the separation of the conjugated RNAs from the sensor surface (at least 1 nm above the GaAs surface), the presence of counterions and the positive charges on the TAT peptides themselves. For example, $Q_{S,\text{RNA}}$ of $-5q$ leads to a surface coverage of 1×10^{12} cm^{-2}, which is quite reasonable given the size of molecules and the associated steric hindrance issues. Hence, it is expected that when biased in the subthreshold regime, an order of magnitude difference in device conductivity is easily possible even with much lower surface coverage (e.g., 1×10^{11} cm^{-2}) of captured TAR RNAs (based on simulation results). Assuming comparable binding efficiency, reduced device dimensions, and allowing enough time for the molecule transport and conjugation kinetics,[19,20] this would correspond to minimum detectable RNA solution concentration of approximately 1–10 nM. Note that biomolecule detection using Si nanowires typically shows a conductivity modulation of 20%–40% and operate at an effective capture efficiency of approximately one target molecule in 4000 nm^2, which is equivalent to the surface coverage of 2.5×10^{10} cm^{-2}.[18] Our results show that with improved surface functionalization techniques, it is indeed possible to achieve extremely sensitive biomolecule detection even when using conventional complementary metal-oxide-semiconductor fabrication techniques, thus enabling the prospects of high density arrays for parallel biomolecule detection. However, the settling time required for a detectable signal change at very low target molecule concentrations is expected to be significantly higher than that of cylindrical nanowire sensors.[19]

IV. CONCLUSION

Label-free electrical detection of the TAT peptide-TAR RNA interaction was demonstrated by using GaAs JFET devices modified with the mixed adlayer of ODT and TAT peptide. The mixed adlayer formed by successive solution-cast self-assembly passivates the GaAs surface from polar ions in buffer solutions while providing selective binding sites for TAR RNA. TAR RNA is recognized by the anchored TAT peptides in the mixed adlayer and induces substantial changes in the device characteristics in terms of pinch-off voltage, subthreshold slope, and hysteresis, which can be correlated with net surface charge density modulation. The JFET devices modified with various thiolated biological species are expected to help elucidate electronic interactions between affixed biomolecules and semiconductor surfaces.

ACKNOWLEDGMENTS

This work was supported in part by NASA under the Institute for Nanoelectronics and Computing (NCC 2-1363) and DARPA/ARO (W911NF-05-0187). We also thank NSF for partial support under Grant Nos. CHE-0614132 and ECS-0506802. The modeling work was performed with financial support from NIH and using computational resources of NCN.

[1] B. M. N. Brinkman and D. T. W. Wong, Curr. Opin. Oncol. **18**, 228 (2006).
[2] N. Tassew and M. Thompson, Anal. Chem. **74**, 5313 (2002).
[3] C.-Y. Zhang, H.-C. Yeh, M. T. Kuroki, and T.-H. Wang, Nat. Mater. **4**, 826 (2005).
[4] G. Zheng, F. Patolsky, Y. Cui, W. U. Wang, and C. M. Lieber, Nat. Biotechnol. **23**, 1294 (2005).
[5] P. S. Waggoner and H. G. Craighead, Lab Chip **7**, 1238 (2007).
[6] P. Bergveld, Sens. Actuators B **88**, 1 (2003).
[7] P. Estrela and P. Migliorato, J. Mater. Chem. **17**, 219 (2007).
[8] Y. Cho and A. Ivanisevic, J. Phys. Chem. B **108**, 15223 (2004).
[9] Y. Cho and A. Ivanisevic, J. Phys. Chem. B **109**, 12731 (2005).
[10] H. H. Park and A. Ivanisevic, J. Phys. Chem. C **111**, 3710 (2007).
[11] C. L. McGuiness, A. Shaporenko, C. K. Mars, S. Jppili, M. Zharnikov, and D. L. Allara, J. Am. Chem. Soc. **128**, 5231 (2006).
[12] F. Seker, K. Meeker, T. F. Kuech, and A. B. Ellis, Chem. Rev. **100**, 2505 (2000).
[13] K. S. Long and D. M. Crothers, Biochemistry **34**, 8885 (1995).

Downloaded 20 Nov 2008 to 128.46.220.88. Redistribution subject to AIP license or copyright; see http://jap.aip.org/jap/copyright.jsp

[14]H. P. Wampler, D. Y. Zemlyanov, K. Lee, D. B. Janes, and A. Ivanisevic, Langmuir **24**, 3164 (2008).
[15]S. M. Sze, *Physics of Semiconductor Devices* (Wiley, New York, 1981).
[16]MEDICI, Two Dimensional Device Simulation Program, Version 2003.06, Synopsis, 2003.
[17]D. McQuarrie, *Statistical Mechanics* (Harper & Row, New York, 1976).
[18]P. R. Nair and M. A. Alam, IEEE Trans. Electron Devices **54**, 3400 (2007).
[19]P. R. Nair and M. A. Alam, Appl. Phys. Lett. **88**, 233120 (2006).
[20]P. R. Nair and M. A. Alam, Nano Lett. **08**, 1281 (2008).

Downloaded 20 Nov 2008 to 128.46.220.88. Redistribution subject to AIP license or copyright; see http://jap.aip.org/jap/copyright.jsp